Bedding-parallel stylolites as a tool to unravel maximum burial depth in sedimentary basins: application to Middle Jurassic carbonate reservoirs in the Paris basin

N. Beaudoin (1,2)*, M. Gasparrini (3), M.-E. David (3,4), O. Lacombe (4) and D. Koehn (2)

(1) Laboratoire des Fluides Complexes et leurs Réservoirs-IPRA, E2S-UPPA, Total, CNRS, Université de Pau et des Pays de l'Adour, UMR5150, Pau, France

(2) School of Geographical and Earth Sciences, University of Glasgow, Gregory Building, Lilybank Gardens, G12 8QQ, Glasgow, UK;

(3) IFP Energies nouvelles, 1 and 4 av. de Bois-Préau, 92852 Rueil-Malmaison, France

(4) Sorbonne Université, CNRS-INSU, Institut des Sciences de la Terre de Paris, ISTeP UMR 7193, F-75005 Paris, France.

*Corresponding author: Nicolas.beaudoin@univ-pau.fr

Keywords: Burial depth, stress inversion, paleopiezometry, stylolites, carbonate reservoirs, Paris basin

Abstract

In recent years stylolites, which are rough dissolution surfaces commonly found in carbonates, have been used for paleopiezometry estimates. The Stylolite Roughness Inversion Technique (SRIT) applied on sedimentary bedding-parallel stylolites (BPS) grants access to the maximum principal vertical stress experienced by the host carbonates and thus to their maximum burial paleo-depth. This study reports the results of SRIT applied to a BPS stylolite population hosted in carbonate platform reservoirs of the Paris basin sub-surface (France). Middle Jurassic carbonates from two well cores from the depocenter and margin of the basin, for which the burial and thermal history are known, based on a thermally calibrated 3D basin model, were analysed. By defining a consistency criterion and using two signal treatment methods, we propose a new approach to select which BPS can be reliably used to reconstruct the maximum vertical stress undergone by the host carbonates, which then can be converted into maximum burial depth. The study of a BPS population shows that there is a control operated by the host rock texture and the stylolite morphology on the burial depth recorded. Especially suture and sharp peak BPS are better suited to estimate the real maximum depth, whereas seismogram pinning BPS record preferentially intermediate depths. Median values of maximum depth derived from our dataset (1.3 and 1.7 km for the margin and depocenter cores, respectively) are in line with maximum burial estimates provided by conventional basin modelling (1450 and 1800 m,

respectively), thus showing that SRIT is a standalone robust depth gauge in sedimentary basins, provided sample selection and data treatment are carried out in a rigorous and thoughtful manner.

1. Introduction

Stylolites are localized rough dissolution surfaces that are encountered in all sedimentary rock types (Alvarez et al., 1978; Koehn et al., 2007) and are particularly common in carbonates, which represent significant host rocks of natural resources (water, oil, gas, ores) worldwide. The chemical compaction process occurring during burial and/or tectonic loading significantly affects the physical properties of carbonate reservoirs by reducing porosity (Raynaud and Carrio-Schaffhauser, 1992; Ehrenberg, 2006). The occurrence of sedimentary stylolites, usually oriented parallel to bedding (bedding-parallel stylolites or BPS) impacts fluid flows, by forming either barriers or drains in reservoir rocks (Koepnick, 1987; Ehrenberg et al., 2006; Hassan, 2007; Heap et al., 2013; Baud et al., 2016; Koehn et al., 2016; Bruna et al., 2018; Martín-Martín et al., 2018, Toussaint et al., 2018). The characteristic teeth of stylolites, oriented oblique or normal to the dissolution surface, are related to the distribution of insoluble elements in the host rock, leading to local pinning under an oriented applied stress (Fletcher and Pollard, 1981; Merino et al., 1983; Koehn et al., 2007). Various genetic models were proposed to account for the initial localization of dissolution along a surface and the lateral propagation of BPS. The pressure-solution model (Merino et al., 1983) considers that stylolites are related to local dissolution under an applied stress field and that the lateral propagation is controlled by the stress concentration at stylolite's tips (anticrack model, Fletcher and Pollard (1981)). This model was questioned by Aharonov and Katsman (2009) because stress concentrations at the tips of a stylolite are relaxed once the stylolite itself supports the applied stress. The clay-enhanced dissolution model (Bjorkum, 1996; Oelkers et al., 1996; Walderhaug et al., 2006), originally developed for quartz-mica interfaces, considers that stylolites develop on a clay-rich interface related to an electrochemical potential at the contact between the host rock and the clay. The clay-enhanced model can explain the localisation of dissolution at a surface and also the lateral propagation of stylolite planes (Aharonov and Katsman, 2009) along clay-rich areas. Both the pressure-solution and the clay-enhanced models can be combined where clay particles, that accumulated during the host rock dissolution under applied stress, enhance the dissolution kinetics (Renard et al., 2001). Since stylolites are features that form during chemical compaction, which is a function of the sediment overburden and since the tooth flanks are parallel to maximum the principal compressive stress, the stress clearly plays a key role in the formation of these features. In carbonates, the type of facies (chiefly dependent on depositional texture, primary mineralogy and abundance of allochems, mud and pores), the morphology (Andrews and Railsback, 1997), the presence of clays and organic matter, as well as the vertical heterogeneity of the strata and the applied stress are the main parameters that govern stylolitization (Shinn and

Robbin, 1983; Bathurst, 1987, 1991; Aharonov and Katsman, 2009; Koehn et al., 2012; Vandeginste and John, 2013; Koehn et al., 2016). Today still, assessing the mechanisms that govern BPS development as well as the quantification of the stress experienced by the stylolite host rock are key points to understand sedimentary basin evolution aiming at improving geological simulations at both the basin and the reservoir scales (Braithwaite, 1988; Andrade Ramos, 2000; Gratier et al., 2005; Peacock and Azzam, 2006; Baron and Parnell, 2007; Benedicto and Schultz, 2010; Angheluta et al., 2012; Koehn et al., 2012; Heap et al., 2013; Khair et al., 2013, 2015; Baud et al., 2016; Bertotti et al., 2017).

In addition to being used to estimate chemical compaction during burial diagenesis (Peacock and Azzam, 2006; Angheluta et al., 2012; Koehn et al., 2016) and to refine deformation history of strata (Benedicto and Schultz, 2010; Tavani et al., 2006, 2015), stylolites have been used to access the magnitude of applied stress. The Stylolite Roughness Inversion Technique (SRIT, Schmittbuhl et al., 2004) is based on a signal analysis of the stylolite's roughness. Successive studies (Renard, 2004; Schmittbuhl et al., 2004; Brouste et al., 2007; Ebner et al., 2009a; Ebner et al., 2009b; Croizé et al., 2010; Ebner et al., 2010a; Rolland et al., 2012, Koehn et al., 2012) established SRIT as a novel paleopiezometric technique, independent from dissolution kinetics, temperature and fluid pressure, that quantifies (1) the maximum vertical stress at the time the dissolution along the stylolite plane stops, and thus the corresponding burial depth, if the method is applied to sedimentary stylolites (Brouste et al., 2007; Ebner et al., 2009b 2010a, 2010b; Rolland et al., 2014; Beaudoin et al., 2016; Bertotti et al., 2017), and (2) the complete stress tensor, by applying SRIT on coeval sedimentary and tectonic stylolites (Ebner et al., 2010a; Rolland et al., 2014; Beaudoin et al., 2016). SRIT relies on the self-affine properties of the stylolite plane roughness to access the magnitude of the stress oriented normal to the stylolite plane (considering a 2D signal, Schmittbuhl et al., 2004) or of both the stresses oriented normal and parallel to the stylolite plane (considering a 3D signal, Ebner et al., 2010b). Even if SRIT was successfully applied to BPS in natural samples and the method reproduced applied external stresses in numerical simulations (Koehn et al., 2012), the magnitudes of the vertical stress reconstructed in published studies show a variability, leading authors to either use averaged values (Bertotti et al., 2017), or to discuss what this variability can mean. Indeed, variable SRIT results were accounted for by considering elastic parameters of the host rock (Rolland et al., 2014), morphological sensitivity of the roughness (Brouste et al., 2007), polyphase burial history or methodological limitations (Beaudoin et al., 2016).

This contribution proposes a statistical appraisal of SRIT applied to a natural BPS population in a weakly tectonized sedimentary basin. Our approach aims at inverting BPS from two cores of the Paris basin sub-surface (Fig. 1) where Middle Jurassic carbonates suffered different maximum burial depth. We

use established signal treatment methods (Simonsen et al., 1998; Renard et al., 2004; Ebner et al., 2009b), Fourier Power Spectrum (FPS) and Average Wavelet Coefficient (AWC), to reconstruct the maximum vertical stress recorded by BPS, and hence the maximum burial depth undergone by the host carbonates. The SRIT is conducted regarding the stylolite morphology, following the recent classification proposed in Koehn et al., (2016), and regarding the depositional texture of the host-rock. On the basis of the direct comparison between the inversion results and the known maximum burial depth independently provided by 3D basin modeling (Fig. 2), we develop a data treatment workflow for BPS populations that show how to use SRIT to access to the maximum burial depth experienced by strata as a reliable paleopiezometer in future studies.

2. Stylolite Roughness Inversion Technique (SRIT)

a. Principles of the technique

SRIT assumes that the stylolite roughness results from a competition between (1) a destabilizing (roughening) force due to pinning particles on the stylolite surface, that resists dissolution in specific locations, locally increasing the Helmholtz free energy and producing peaks and teeth; and (2) two stabilizing (smoothening) forces, long-range elastic forces and local surface tension, that tend to reduce the Helmholtz free energy of the solid, leading to flattening of the surface by localizing dissolution on areas of local roughness (Schmittbuhl et al., 2004; Koehn et al., 2007, Rolland et al., 2012). The stylolite roughness displays self-affine properties, i.e., a geometry that is invariant across a range of scales typically with a different scaling in x than in y so that the surface becomes rougher towards smaller scales. The two stabilizing forces are efficient at different spatial scales so that two regimes can be defined: an elastic energy-dominated regime at a large-scale (above mm, typically), and a surface energy-dominated regime at a small-scale (below mm, Schmittbuhl et al., 2004). Each of the stabilizing forces is characterized by a specific roughness coefficient (called Hurst coefficient) that can be determined by conducting a Fast Fourier Transform, Wavelet Analysis or applying a Correlation Function on the roughness profile along a stylolite. This Hurst coefficient has been extensively documented in natural stylolites (Brouste et al., 2007), and the transition from one stabilizing force spatial scale domain to the other is called the crossover length (Lc). Lc is related to both the mean stress and differential stress the rocks sustained during stylolite growth according to Schmittbuhl et al. (2004)

$$\mathrm{Lc} = \frac{\gamma \mathrm{E}}{\beta \sigma_{\mathrm{m}} \sigma_{\mathrm{d}}}, \quad (1)$$

where the cross-over length Lc (mm) is linked to the Young's modulus E (Pa), to the solid-fluid interfacial energy γ ($J.m^{-2}$), to the dimensionless constant $\beta = \upsilon(1-2\upsilon)/\pi$ with υ being the Poisson's ratio, and to the mean and differential stress, σ_m and σ_d, respectively. It is noteworthy that this

equation is valid considering that the stylolite localized along a water-rock interface, and that the mechanical properties of the dissolved rock remain constant during dissolution. Provided the rock properties are known, SRIT therefore grants access to the stress acting normal to the BPS plane.

b. Measurement methodology

The roughness signal was studied following the approach described in Schmittbuhl et al. (2004) and Ebner et al. (2009b). Surfaces of core samples, cut perpendicular to the stylolite planes, were hand-polished using abrasive grinding papers from coarse (250 µm) to extra fine (2.5 µm) allowing gentle polishing in order to prevent any alteration of the material. Once the stylolite track visually contrasts with the host rock, the surface is scanned in 2D at a resolution of 12800 dpi. Stylolite tracks were hand-drawn using a drawing software (GIMP) with a 5 pt. thick line. We then used scripts presented in Ebner et al. (2009b) to rotate the stylolite plane back to horizontal. The resulting 1D signal was analyzed using the Fourier Power Spectrum (FPS; Renard et al., 2004) and the Average Wavelet Coefficient (AWC) methods with Daubechies D4 wavelets (Simonsen et al., 1998; Ebner et al., 2009b). Both methods have been applied to roughness 1-D profiles, and returned similar results (Simonsen et al., 1998; Candela et al., 2009; Ebner et al., 2009b). The general signal analysis resolves around the self-affine properties of the stylolite roughness, defined as the height difference Δh between two points of the rough surface separated by a distance Δx. A self-affine signal is characterized by $\Delta h \approx \Delta x^H$, where H is the Hurst coefficient. In the case of a FPS analysis, in which the signal is considered as a sum of periodic sinuses and cosinuses, the wave number k (mm^{-1}) and the squared Fourier transform modulus P(k) are related as $P(k) = k^{2H+1}$. In the case of an AWC analysis, in which the signal is reconstructed in a sum of different wavelets, starting with a mother function (Simonsen et al., 1998), the scale a (mm) and the averaged wavelet coefficient W(a) are related as $W(a) = a^{H+0.5}$. For each method, it is possible to access the H coefficient based on the slope that links the data, picked following a binning interval, on a log-log plot, and using the relations reported above. In an ideal case, two straight lines should be traceable on log-log plots, a steep line at the lower scale values, characterized by a H of 1 (corresponding to surface energy), and a gentle slope line at the higher scale values, characterized by a H of 0.5 (corresponding to elastic energy). The observation scale (k for FPS, a for AWC) at which the two slopes intersect is the crossover length Lc that is related to the vertical stress for sedimentary stylolites. In order to reduce uncertainty on Lc, we fit the line that goes through the maximum of binned data points and use slopes that satisfy the theoretical H coefficients. To estimate the error on the Lc value obtained, we consider a domain of transition between the two regimes using the scale at which there is a clear separation of the two slopes on each side of the intersection (log-log plots of Fig. 6). This domain represents an error graphically evaluated from ±4% to ± 10% of the Lc, depending

on where the Lc sits on the log-log plot. It is noteworthy that the SRIT is independent of the dissolution kinetics, the surrounding fluid pressure and the amount of dissolution. Thus, the amount of chemical compaction accommodated by the stylolites is beyond the scope of this study.

c. BPS inversion for vertical stress and depth assessment

For BPS, we can assume a zero horizontal displacement in the stylolite plane, corresponding to a perfect isotropy of the horizontal principal stress, such as $\sigma_v > \sigma_H = \sigma_h$ (σ_H and σ_h are the notation for the maximum and minimum horizontal principal stress, respectively), leading to the simplification of the equation (1) as:

$$\sigma_v^2 = \frac{\gamma E}{\kappa Lc} , \quad (2)$$

with $\kappa = \frac{\nu}{3\pi} \times \left(\frac{(1-2\nu)^2(1+\nu)}{(1-\nu)^2}\right)$ (Koehn et al., 2012). Finally, the depth h is obtained using $\sigma_v = \rho g h$, with ρ the rock density and g the gravitational field acceleration. In our study, we use the classic solid-fluid interfacial energy value for calcite (ν=0.27 J.m^{-2}), the averaged mechanical parameters obtained from mechanical testing conducted on the Comblanchien carbonate formations (Bemer and Lombar, 2010): a Poisson's ratio of 0.22, a Young's modulus of 34 GPa, and a density for carbonates of 2700 g.cm^{-3}. Considering the error on the Lc values, and the range of the mechanical parameters (E = [31 – 36] GPa, Poisson's ratio [0.21-0.23]), the uncertainty on the inversion results is ±10 %.

3. Case study of the Middle Jurassic carbonates of the Paris basin

a. Geological and thermal history

The Paris basin is a Meso-Cenozoic intracratonic basin which initiated in late Carboniferous and Permo-Triassic times in response to the extensional collapse of the thickened Variscan lithosphere and reactivation of inherited Variscan structures (Perrodon and Zabek, 1990; Guillocheau et al., 2000; Le Solleuz et al., 2004; Averbuch and Piromallo, 2012). It is mainly filled by Mesozoic sediments lying uncomformably on a Paleozoic basement (Fig. 1), with the whole sedimentary column (from Triassic to Tertiary) reaching about 3000m of thickness in the central part of the basin (Fig. 1). During Mesozoic times the Paris basin experienced a simple burial history, punctuated by periods of rapid subsidence in the Jurassic and Late Cretaceous and of minor uplifts. A major tectonic inversion occurred at the Mesozoic-Cenozoic boundary, which led to the main uplift phase causing the exposure of the entire basin (Brunet and Le Pichon, 1982; Guillocheau et al., 2000; Barbarand et al., 2013). At the southern and eastern basin margins evidence for three Cenozoic tectonic events were recorded: the Pyrenean orogeny (N-S compression; Eocene), the opening of the Bresse and Rhine grabens related to the West European Rifting (E-W to WNW-ESE extension; late Eocene – Oligocene) and the Alpine orogeny

(WNW-ESE compression; Miocene-Pliocene) (Lacombe et al., 1990, 1993, 1994; Guillocheau et al., 2000; Andre et al., 2010).The sedimentary succession has been extensively explored for oil and gas resources (Espitalié et al., 1988; Delmas et al., 2002, 2010), which migrated mostly in Late Cretaceous time into reservoir rocks from different stratigraphic intervals (mainly Upper Triassic, Middle Jurassic and Lower Cretaceous; Wendebourg and Lamiraux, 2002; Delmas et al., 2002, 2010).

In this study, a 3D basin model for the Paris basin was used to extract the burial and thermal history of the studied cores. The original geometric model was constructed with the TemisFlow software for basin modeling, (Teles et al., 2014) and was recently improved by considering a lithospheric model for heat transfer, and by reconstructing paleobathymetry maps and eroded thicknesses through time (Torelli, 2018) (Fig. 2). Thermal calibration was accomplished with present-day bottom hole temperatures (BHT) and conventional organic thermometers, like vitrinite reflectance and Rock-Eval pyrolysis data (Torelli, 2018). Further constraints were also made available from absolute thermo-chronometry of carbonate cements from the same stratigraphic unit studied here (Mangenot et al., 2017; Mangenot et al., 2018).

b. Studied sedimentary cores

This study focuses on the sedimentary, bedding-parallel stylolite (BPS) population hosted in two exploration well cores, one from the depocenter (Rigny-la-Nonneuse; hereafter referred as Rigny) and one from the southern margin (Parly) of the basin (Fig. 1). The stratigraphic interval studied consists of the Upper Bathonian – Lower Callovian platform carbonates corresponding to the *Comblanchien* and *Dalle Nacrée* Fms., separated by a major transgressive surface (Guillocheau, 1991; Guillocheau et al., 2000) and differentiated based on their biostratigraphic content (Garcia, 1993; Garcia and Sambet, 1994). This corresponds to a large isolated platform, recording no detrital input from the continent. The two cores exhibit a different thermal and burial history (Fig. 2). Currently, the studied interval is buried at a depth of 1537-1574 m in the basin depocenter (Rigny) and at a depth of 640-663 m on the basin southern margin (Parly). The 3D model further predicts that at peak burial conditions the Middle Jurassic carbonates experienced depths of 1800 m and 1450 m and temperatures of 92 and 80 °C in the Rigny and Parly cores, respectively (Fig. 2). Figure 2 also illustrates that the carbonates experienced a simple burial history characterized by a nearly continuous burial until Late Cretaceous, followed by a main uplift event. Thus, the rocks mainly underwent normal overburden pressure (inducing development of BPS) and escaped major tectonic deformations.

The Upper Bathonian – Lower Callovian stratigraphic interval investigated is 37 and 23 m thick in the Rigny and Parly cores, respectively. Sedimentary logging and macro-facies analysis were accomplished

at the 1:100 scale and sampling for thin section preparation and petrographic micro-facies analysis was performed on average every 1 m of core and specifically in close vicinity of the BPS selected for SRIT analysis (Fig. 3a). Gas and water porosimetry on this stratigraphic interval at basin scale revealed a wide range of porosities from 0 to 22%, with average and mode values that are 5.5% and 3-4%, respectively (Delmas et al., 2010). However, 2D point counting estimates on thin sections from the studied cores point towards porosity mostly below 5% (Mangenot et al., 2018).

Macro- and micro-facies analyses and comparison with previously published works (Gaumet, 1994, 1997; Granier, 1995; Gaumet et al., 1996) allowed us to distinguish a total of 23 carbonate facies from the two studied cores. Based on sedimentary structures, depositional textures, as well as type and proportion of allochems, mud and primary pores, the 23 facies were ascribed to 6 depositional environments (Fig. 4): (1) Intertidal deposits are mainly composed of packstone and grainstone dominated by intraclasts (1-10 mm) and reworked oncoids (0.5-1.5 cm) with oblique lamination and fenestral pores, typical of high energy sediments subjected to periodic emersions; (2) Sub-tidal lagoon deposits are mainly composed by wackstone to packstone dominated by oncoids, locally reaching 2 cm in diameter (floatstone), and peloids, associated with planar microbial mats, suggesting a low to medium energy environment; (3) Deep lagoon deposits are mainly composed of mudstone and wackstone containing small (<1 mm) oncoids, locally associated with lenses of organic-rich sediments, indicating a very low energy environment; (4) Back-shoal to shoal deposits. The former are mainly composed of the lagoonal facies containing spill-over deposits derived from the shoal. The latter include high energy grainstone and packstone composed of ooids (<2mm), coated grains (1-2 mm), peloids (<0.5 mm), bioclast fragments (crinoids, corals, bryozoans, brachiopods, bivalves) locally with cross-stratification and rare evidences of emersion associated with geopetal features and fenestral pores; (5) Fore-shoal deposits include mud-, wack-, pack- and grainstone with dominant peloids (<0.5 mm) and bioclast fragments (mainly crinoids, brachiopods and bivalves) and encrusting serpulids; (6) Off-shore deposits include wackstone with wavy bedding containing few crinoid fragments (<0.5 mm), commonly recrystallized and locally associated with dark lenses of clay-size particles (organics or siliciclastics), deposited in a low energy setting.

Petrographic analysis did not identify phyllosilicates like micas in any of the 23 sedimentary facies. Minor clay-size particles, likely siliciclastic, were identified only in the off-shore environment and are possibly linked to upwelling from distal plains, whereas clay-size particles, likely organic, were identified in the deep lagoon environment where anoxic conditions could have favoured their preservation.

For the scope of this survey the 23 facies identified were gathered into 4 main groups based on the dominant carbonate textures (*sensu* Dunham, 1962) irrespective of the depositional environment of provenance: (1) Mudstone to wackstone (locally with clay-size siliciclastic and organic particles) with minor oncoids, peloids and bioclast fragments (<0.5 mm); (2) Wackstone to floatstone mainly with oncoids, peloids and locally intraclasts (<2 mm); (3) Floatstone to packstone with oncoids, intraclasts and locally peloids (1.5 cm); (4) Packstone to grainstone with ooids, coated grains, intraclasts, bioclasts (mainly brachiopods and crinoids) and locally oncoids (up to 2 cm). These groups will be further used to assess the role of the carbonate depositional texture on the results of SRIT analysis.

c. Stylolite populations

Stylolite populations in the cores consist exclusively of bedding-parallel stylolites (BPS) that formed in response to vertical stress during burial (Fig. 3b), in a setting where the horizontal stress is likely to remain isotropic. All peaks are observed normal to the stylolite planes, indicating that the governing stress direction was vertical (Koehn et al., 2012), and that no horizontal displacement occurred along the stylolite plane. The investigated core samples were typically 15-20 cm long (Fig. 3b). Twenty-five (25) samples (core slabs) containing single-trace stylolites were considered for the SRIT, and forty-eight (48) stylolites were selected with lengths ranging from 1.5 cm to 7.4 cm. Sampling covers different depositional facies and corresponding environments in both cores (Fig. 3a), comprising 14 samples (32 stylolites) from the Parly core (covering the 643-663 m depth interval) and 11 samples (16 stylolites) from the Rigny core (covering the 1542-1559 m depth interval), respectively. Stylolites were characterized regarding their morphologies, following the classification proposed by Koehn et al. (2016). This classification comprises 4 classes of stylolites based on the shape of the roughness, which itself is related to the stylolite growth (Fig. 5). In the following description the stylolite morphology is split into a baseline corresponding to above-mm scale morphology and peaks referring to below-mm scale morphology. Class 1 stylolites (rectangular layer) consist of a large rectangular baseline with small peaks on the rectangle flat top. Class 2 stylolites (seismogram) are characterized on the large scale by the occurrence of narrow top-hat like rectangles, with small-scale peaks. Class 3 (suture and sharp peak) includes all stylolites that have a flat or wavy base line with locally tall peaks. Finally, Class 4 stylolites (simple wave) display a wavy base line and sparse small peaks. Numerous core samples comprise stylolites with various morphologies, indicating that the morphology is independent from the depositional textures/facies and corresponding environments. A rough minimum estimate of the vertical displacement (compaction) that the studied stylolites accommodated can be obtained by measuring the maximum amplitude of the teeth along the 2D profile (Koehn et al., 2016, Toussaint et al., 2018). These amplitude values are reported in the Table 1, showing stylolites accommodated a minimum of 1.14 mm to 8.4 mm vertical displacement.

Superposition of stylolite teeth also suggests a complex polyphase development of pressure-solution in the strata, and the anastomosed pattern results from complex interactions between stylolite planes that likely destroyed the original roughness (Sinha-Roy, 2002; Laronne Ben-Itzhak et al., 2014). Consequently, we discarded overprinted or fused stylolites from our study so that SRIT analysis focussed on single, isolated stylolites only.

4. SRIT results

The roughness of forty-eight (48) stylolites was studied using both the FPS and AWC methods (Table 1). Figure 6 shows representative examples of the obtained treatment. By calculating the values of the Hurst coefficient for each stylolite, we can divide the population into three categories: (1) stylolites of which both small-scale and large-scale Hurst coefficients correspond to 1±0.1 and to 0.5±0.1, respectively. These values are the theoretical ones expected from the growth model (Schmitbuhll et al., 2004), and we consider an uncertainty of ±0.1 to account for user-related sources of error (stylolite drawing and value reading mainly, Fig. 6a). Thirty-five and twenty-six stylolites satisfy this criterion when analysed using AWC and FPS, respectively; (2) stylolites of which either one or both small-scale and large-scale Hurst coefficients do not correspond to the theoretical values (Fig. 6b). Eight and thirteen stylolites belong to this category, when analysed using AWC and FPS respectively; (3) stylolites where roughness analysis does not show two growth regimes, hence no cross-over length (Fig. 6c). Five and eight stylolites belong to this category, when analysed using AWC and FPS, respectively. The fact that both small-scale and large-scale Hurst coefficients reconstructed satisfy the theory is the key factor to select the stylolites among the population that are the best suited to be used as paleopiezometers. This characteristic is hereafter referred to as the consistency.

In order to characterize the stylolites that are the best suited to be used for SRIT, we studied the statistical distribution of the population considering the consistency with the growth model, the stylolite morphology and the host rock texture. Vertical stress and corresponding burial depth distribution modes (first and third quartiles and median) of the population were compared to the depth predicted by the burial-thermal modelling. This approach enables us to establish the most efficient way to use SRIT to access the maximum depth experienced by the strata on one hand, and to assess the impact of the stylolite morphology or of the host rock texture on the other hand. It is worth noting that the results from SRIT analysis are more consistent with the modelled depths when analyzed using the AWC method rather than the FPS method.

To account for the difference in the depth estimates depending on the signal analysis method used, we considered FPS and AWC averaged depth values for the stylolites that are referred to as consistent, i.e. those with Hurst coefficients consistent with Schmittbuhl et al. (2004). More than 80% of the

stylolites satisfy the consistency criterion in our sample population, considering either results from AWS, or from FPS or from both, the latter case encompassing 50% of the whole population. The depth median value obtained from the average between FPS and AWC inversion for these stylolites is very close to the maximum burial depth predicted by the burial-thermal model (Figs. 2 and 7). Indeed, SRIT returns maximum depths of 1300 ± 100 m for the Parly core and 1650 ± 100 m from the Rigny core, while maximum depths estimated by the basin model are 1450 m in Parly and 1800 m in Rigny. This shows that the depth median value derived from a stylolite population can be used to reliably access the maximum burial depth, provided stylolites satisfy the consistency criterion previously defined in this study.

5. Discussion

a. Impact of the stylolite morphology on SRIT reliability

Sedimentary rocks host stylolites of various morphologies, which can be described based on teeth frequency, wavelength and amplitude at different observation scales (Andrews and Railsback, 1997). Stylolite morphology affects estimates of the chemical compaction and the efficiency of fluid flow along the dissolution planes (Braithwaite, 1988; Meredith et al., 2011; Heap et al., 2013; Koehn et al., 2016). Morphology is likely to be controlled by both the growth regime (Koehn et al., 2016) and the host rock heterogeneity distribution such as porosity (Andrews and Railsback, 1997) or pinning particles (Koehn et al., 2007; 2012). Both these parameters deeply affect the ability of a stylolite to record two-scales of growth regimes, hence reliable stress magnitudes (Renard, 2004; Ebner et al., 2009b; Ebner et al., 2010a; Ebner et al., 2010b; Rolland et al., 2014). The case study of the Middle Jurassic carbonates from the Paris basin subsurface enables us to discuss how reliable the SRIT is with respect to the stylolite morphology. We studied stylolites clearly related to the vertical stress applied, with teeth oriented vertical and perpendicular to the dissolution plane, and formed in rocks containing very few clays and no micas. In order to assess whether morphology plays a noticeable role on the SRIT results, we reported a statistical analysis of the BPS populations as box-and-whisker plots as a function of the morphology (Fig. 8a). It is worth noting that provided that the stylolite 2D profile is long enough for both the roughness Hurst exponents to be found (>1.5 cm, Table 1), our dataset shows that SRIT returns a Lc independent from the stylolite length and from the amount of vertical displacement it accommodated. Also no correlation can be found between 2D profile length and the validation of the consistency criterion.

SRIT results vary depending on the stylolite morphology (classes 2, 3 and 4, Fig. 8a): stylolites from class 2 are systematically underestimating the maximum burial depth, with median values ranging between 1000 and 1150 m, and up to 65% of the population satisfying the consistency criterion.

Stylolites from class 3 return a depth in line with the estimated maximum burial depth (1350 m – 1600 m) and up to 80% of the population is consistent with the depths derived from burial-thermal model (Fig. 2). Stylolites from class 4 show the most scattered distribution, with no systematic behaviour regarding the depth, suggesting they are not the best suited to obtain a reliable depth estimate, despite 75% of them satisfying the consistency criterion. Stylolites belonging to class 3 seem to be the best suited to calculate the maximum burial depth, while class 2 stylolites are better indicators of intermediate depths. We suggest avoiding the simple wave-like stylolites (class 4), which will not return a reliable depth, probably because of the lack of teeth, most of the signal then relying in a small-scale roughness which is difficult to digitize and so to analyse.

b. Impact of the host rock depositional texture on SRIT reliability

The texture of the host also seems to affect the inversion results (Fig. 8b), with consistent results for the 4 textures documented. Texture 1 (mudstone to wackstone) returns the most scattered depth distribution, with 75% consistency, and a clear difference in the median value for FPS (1100m) or for AWC (1700m). Texture 2 (wackstone to floatstone) hosts stylolites that return a narrow depth distribution (1400 to 1650m) in the range of the depths expected from the burial-thermal model considering both cores, and 100% consistency. Textures 3 (floatstone to packstone) and 4 (packstone to grainstone) host stylolites of which quartile distribution is narrow (1000 to 1400 m), with median values slightly underestimating the maximum burial depth modelled with a consistency of 90% for texture 3 and of 50% for texture 4. From this statistical representation, it returns that wackstone, floatstone and packstone are the better suited host rock textures to assess the maximum burial depth, grainstone hosting more than half of the inconsistent stylolites, and mudstone being the less suited texture to assess a burial depth, should it be maximum or intermediate.

c. Limitations of SRIT and application beyond the case of sedimentary basins

The application of SRIT requires a good estimate of mechanical parameters (young modulus and poison ratio) and of the solid-fluid interfacial energy. If the latter is strictly related to the host lithology and does not vary much with the conditions of deformation (compaction, temperature, pressure), mechanical parameters are likely to evolve as the host undergoes shortening or compaction, as emphasized in Rolland et al. (2012). The Young's modulus E is the most critical parameter to assess, and determining it at the time of the deformation is not trivial. One solution was proposed by Ebner et al. (2009b), that uses the SRIT results carried on several BPS hosted in the same rock to assess the value of E prevailing at the time stylolites formed. The method inverts equation (2), using the difference in vertical stress from BPS separated by a measured distance to access E. In cases where the studied succession is not long enough to apply this approach (i.e. <10 m), a minimum requirement

to carry out SRIT is to know the value of E from mechanical tests (e.g. this paper). It is important to be aware of these limitations when assessing vertical stress in deep conditions of deformation, or in different lithologies. In addition, the SRIT presented in this paper is tied to the assumption that the stress in the plane of the stylolite is isotropic. It is very likely that the horizontal stress remained isotropic in settings with very limited shortening or extension like the subsidence phase of the Paris Basin, however in other settings where SRIT was successfully applied such as foreland basins this isotropy may not be valid (Beaudoin et al., 2016; Bertotti et al., 2017; Beaudoin and Lacombe, 2018). In such settings, it appears important to check that the horizontal stress remained isotropic for a given BPS, (1) by ensuring the teeth are perpendicular to the dissolution plane (so that the surface contains no shear component) and (2) testing a sample with SRIT applied to a stylolite in three cuts at 60 degrees to each other that should return identical values for Lc, as anisotropy in stress creates an anisotropy of the Lc values (Ebner et al., 2010b). Otherwise, alternative approaches exist for anisotropic stresses along the stylolite plane, which typically occurs for tectonic stylolites (Ebner et al., 2010b; Beaudoin et al., 2016).

Formational fluids involved in the pressure-solution process have a strong impact on stylolite development (Toussaint et al., 2018, and reference therein). In order to test the impact of fluids onto SRIT, we consider the paleo-fluids circulating within the Middle Jurassic reservoirs of the Paris basin, assessed on several cores from the basin depocenter and margin (including Rigny core, Mangenot et al., 2017, 2018; Dassié et al., 2018). The studied interval in the Rigny core consists in a highly saline-dominated fluid system during the whole burial time (Cretaceous), yet various vertical stresses were reconstructed by applying SRIT on this interval. Consequently, it suggests that the pore fluid chemistry is not affecting the SRIT results. Also, the study of both Parly and Rigny cores illustrates that the occurrence of oil migration at maximum burial, observed in Rigny but absent from Parly, does not impact the SRIT result in spite of being able to affect stylolite development. This highlights that the external parameters such as fluid chemistry or environment temperature affect stylolite development (reviewed in Toussaint et al., 2018) but are not involved in SRIT equations and do not affect the SRIT results.

d. Lessons learnt on sedimentary stylolite development

The study from the Middle Jurassic carbonates of the Paris basin highlights that 80% of the stylolite population is consistent with the growth model, hence that they are suitable for SRIT. 20% of the population of stylolites fails to return consistent Hurst coefficients with both methods. This failure takes two shapes: (1) a single growth regime, always related to the surface energy scale, in which case it is safe to assume that the 2D portion is too small to encompass where the Lc sits, emphasizing that

the 2D stylolite used for SRIT must be longer than the Lc by at least two orders of magnitude, or (2) 2 growth regimes, but the Hurst exponent being different from what the model predicts. In that case, the roughness may have been altered during chemical compaction either by excessive pinning, an effect that is especially visible in morphology classes 1 and 2 (Koehn et al., 2007; Ebner et al., 2009a), or by a transient stop in the dissolution history, altering the roughness and Hurst exponent of the large-scale elastic energy (Laronne Ben-Itzhak et al., 2014).

Half of the stylolites that show consistency with the growth model stopped developing at an intermediate depth, returning an intermediate vertical stress value. The results of SRIT suggest two possible scenarios to account for the development of stylolites that do not finish their growth at the same depth: (1) all stylolites start dissolution at the same time, some stopping before others. (2) stylolites start dissolution in sequence, class 2 forming and stopping, then class 3 forming and stopping. The depth distribution shown in Figure 8a seems to support the latter case. However, such a scenario requires that there is enough space in between dissolving stylolites to localize new ones. As the dissolution increases during burial, the spacing between stylolites tends to decrease, because of the physical effect of dissolution on the one hand, and because of the effect of increasing vertical stress coupled to an increase in local fluid pressure (Kelka et al., 2017) due to a decrease in local permeability around the stylolite (Koehn et al., 2016). Thus, it is physically unlikely that sedimentary stylolites developed in sequence (class 2 then 3) and it is more sound to consider that all dissolution planes start at the same time, with some stylolites stopping before others.

Our study shows that the seismogram pinning type morphology (class 2) statistically yields a fossil stress signal that corresponds to an intermediate burial depth (Fig 9). Alternatively, the suture and sharp peak type morphology (class 3), where pinning is distributed along the plane, tends to record the maximum burial depth-related stress, suggesting that growth and so dissolution were active until the maximum burial depth was reached (Fig. 9). This suggests that the strong localized pinning can kill the roughness ability to record deep stress. The role of pinning may govern the impact of host texture on SRIT results, i.e. that coarser grained texture returns intermediate values of vertical stress (Fig. 8). Indeed, if we do not expect that heterogeneous grain size distribution in a sample would affect SRIT, the range of grain sizes in a homogeneous sample will control the distribution of the pinning particles (e.g. oxydes). In a rock with coarser grains like a grainstone, pinning particles will be further apart from each other, and so the pinning will be localized in those points, leading to a shorter lifespan of the stylolite. This idea corroborates the observations of Andrews and Railsback (1997), that reported that more serrate stylolites (class 1 and 2 here) seem to predate less serrate stylolites (class 3). Authors related this to the development of stylolites in sequence, affected by the evolution of the rock lithology with burial, where destruction of porosity and decrease in amount of heterogeneities tends

to decrease the pinning effect. We propose that this observation rather reflects that most BPS initiated at the same time, with the more serrate stylolites stopping their development earlier then the less serrate stylolites because of the localized pinning, itself controlled by the distribution of pinning particles in the rock (Koehn et al., 2012). Our study also reports that the minimum burial depth recorded by a BPS at the time it stopped developing is 800 m, which suggests that dissolution started at lower depth. That supports the studies reporting sedimentary stylolites developing at very shallow depth (150m, e.g. Rolland et al., 2012), and contradicts the previous attempts to infer a minimum burial depth needed for stylolite formation (from 800 m to 1000 m, Finkel and Wilkinson, 1990; Railsback, 1993; Dunnington, 1967; Nicolaides and Wallace, 1997). Our study results suggest that a combination of SRIT applied on classes 2 and 3 stylolites in carbonate rocks, considering each stratigraphic unit as hosting a population, can be used to reconstruct a major part of the basin subsidence history.

6. Conclusions

Using two cores from Middle Jurassic carbonate reservoirs of the Paris basin (France), of which the burial-thermal history is well constrained, this contribution presents a first statistical appraisal of the Stylolite Roughness Inversion Technique (SRIT) applied to sedimentary, bedding-parallel stylolites (BPS) aiming to access maximum paleo-depth experienced by their host rocks. By direct comparison between inversion results and modelled maximum burial depths, we define a mathematical consistency criterion, fulfilled if stylolite roughness analysed with either the Fourier Power Spectrum (FPS) or the Average Wavelet Coefficient (AWC) methods returns 2 growth regimes with Hurst coefficient of 1±0.1 for the surface energy (typically encountered at a scale below 1 mm) and 0.5±0.1 for the elastic energy (above 1 mm). Then, the median values of the depth considering the stylolites consistent with the growth model approach the maximum burial depths giving 1300m ± 130 m for the southern margin core and 1650m ± 160m for the depocenter core. These values are close to (within 10%) those independently deduced from a thermally calibrated basin model, yielding maximum paleo-depths for the studied carbonates of 1450 and 1800 m, respectively.

From a distribution analysis, we assess the impact of stylolite morphology and host rock depositional texture on the reliability of SRIT, and we propose that suture and sharp peak stylolite types are the best suited to access the maximum paleo-depth, while the seismogram pinning type provides intermediate depth values. This survey encourages future basin studies to use SRIT since a moderate number of stylolites (<5) is needed to consistently return the maximum burial depth, or an intermediate burial depth, provided that a selection of the stylolites based on their morphology is

properly made and that the Hurst coefficient consistency is respected. In cases where such selection proves to be hard, we suggest that future studies should avoid using the simple wave-like stylolites and the mudstone host rock textures, since both show the largest variability on SRIT results. We also suggest to work on a population of a minimum of 15 stylolites to obtain a reliable estimate of the maximum depth.

Beyond presenting a workflow to assess the maximum burial depth from BPS population, our study points out that nearly 100% of the sedimentary, bedding-parallel stylolites developed in accordance to the stress-driven growth theory that links the stylolite roughening to the applied stress. 80% of the studied population retain this relationship intact. We propose that BPS development starts from the same depth (≤ 800 m), with localized strong pinning tending to stop the dissolution at intermediate depths during burial. Thus only the stylolites where pinning is distributed along the plane can yield the maximum vertical stress magnitude.

Acknowledgements

The authors would like to thank R. Wells and R. Toussaint for their constructive reviews. The subsurface cores of Rigny-la-Nonneuse and Parly were available from the IFPEN storage collection of the BEPH (*Bureau Exploration-Production d'Hydrocarbures*). Fabrice Gaumet (Terramelior) is thanked for valuable advice during sedimentary logging of the cores.

References

Aharonov, E., and Katsman, R., 2009, Interaction between pressure solution and clays in stylolite development: Insights from modeling: American Journal of Science, v. 309, p. 607-632, http://doi.org/10.2475/07.2009.04.

Alvarez, W., Engelder, T. and Geiser, P.A., 1978, Classification of solution cleavage in pelagic limestones: Geology, v. 6, p. 263-266.

Andrade Ramos, J.R.D., 2000, Stylolites: Measurement of Rock Loss: Revista Brasileira de Geosciências, v. 30, p. 4.

Andre, G., Hibsch, C., Fourcade, S., Cathelineau, M. and Buschaert, S., 2010, Chronology of fracture sealing under a meteoric fluid environment: Microtectonic and isotopic evidence of major Cainozoic events in the eastern Paris Basin (France): Tectonophysics, v. 490, p. 214-228.

Andrews, L. M., and Railsback, L. B., 1997, Controls on stylolite development: morphologic, lithologic, and temporal evidence from bedding-parallel and transverse stylolites from the US Appalachians: The Journal of Geology, v. 105, no. 1, p. 59-73.

Angheluta, L., Mathiesen, J. and Aharonov, E., 2012., Compaction of porous rock by dissolution on discrete stylolites: a one-dimensional model: Journal of Geophysical Research, v. 117, p. 8, http://doi.org/10.1029/.

Averbuch, O., and Piromallo, C., 2012, Is there a remnant Variscan subducted slab in the mantle beneath the Paris basin? Implications for the late Variscan lithospheric delamination process and the Paris basin formation: Tectonophysics, v. 558, p. 70-83.

Barabási, A.-L., and Stanley, H.E., 1995, Fractal concepts in surface growth: Cambridge university press, 366 p.

Barbarand, J., Quesnel, F., and Pagel, M., 2013, Lower Paleogene denudation of Upper Cretaceous cover of the Morvan Massif and southeastern Paris Basin (France) revealed by AFT thermochronology and constrained by stratigraphy and paleosurfaces: Tectonophysics, v. 608, p. 1310-1327.

Baron, M., and Parnell, J., 2007, Relationships between stylolites and cementation in sandstone reservoirs: Examples from the North Sea, U.K. and East Greenland: Sedimentary Geology, v. 194, p. 17-35, http://doi.org/10.1016/j.sedgeo.2006.04.007.

Bathurst, R.G., 1987, Diagenetically enhanced bedding in argillaceous platform limestones: stratified cementation and selective compaction: Sedimentology, v. 34, p. 749-778.

Bathurst, R.G., 1991. Pressure-dissolution and limestone bedding: the influence of stratified cementation, *in* Einsele, G., Ricken, W., and Seilacher, A., eds., Cycles and Events in Stratigraphy: Springer [Berlin], p. 450–463.

Baud, P., Rolland, A., Heap, M., Xu, T., Nicolé, M., Ferrand, T., Reuschlé, T., Toussaint, R., and Conil, N., 2016, Impact of stylolites on the mechanical strength of limestone: Tectonophysics, v. 690, p. 4-20, http://doi.org/10.1016/j.tecto.2016.03.004.

Beaudoin, N., and Lacombe, O., 2019, Recent and future trends in paleopiezometry in the diagenetic domain: Insights into the tectonic paleostress and burial depth history of fold-and thrust belts and sedimentary basins: Journal of Structural Geology, https://doi.org/10.1016/j.jsg.2018.04.001 (in press).

Beaudoin, N., Koehn, D., Lacombe, O., Lecouty, A., Billi, A., Aharonov, E., and Parlangeau, C., 2016, Fingerprinting stress: Stylolite and calcite twinning paleopiezometry revealing the complexity of progressive stress patterns during folding-The case of the Monte Nero anticline in the Apennines, Italy: Tectonics, v. 35, p. 1687-1712, http://doi.org/10.1002/2016tc004128.

Bemer, E., and Lombard, J. M., 2010, From injectivity to integrity studies of CO2 geological storage-chemical alteration effects on carbonates petrophysical and geomechanical properties: Oil & Gas Science and Technology–Revue de l'Institut Français du Pétrole, v. 65, no 3, 445-459.

Benedicto, A., and Schultz, R.A., 2010, Stylolites in limestone: Magnitude of contractional strain accommodated and scaling relationships: Journal of Structural Geology, v. 32, p. 1250-1256, http://doi.org/10.1016/j.jsg.2009.04.020.

568 Bertotti, G., de Graaf, S., Bisdom, K., Oskam, B., Vonhof, H.B., Bezerra, F.H., Reijmer, J.J., and Cazarin,
569 C.L., 2017. Fracturing and fluid-flow during post-rift subsidence in carbonates of the Jandaíra
570 Formation, Potiguar Basin, NE Brazil: Basin Research, v. 29, p. 836-853.

571 Bjorkum, P.A., 1996, How important is pressure in causing dissolution of quartz in sandstones?:
572 Journal of Sedimentary Research, v. 66, p. 147-154.

573 Braithwaite, C.J.R., 1988, Stylolites as open fluid conduits: Marine and Petroleum Geology, v. 6, p. 93-
574 96.

575 Brouste, A., Renard, F., Gratier, J.-P., and Schmittbuhl, J., 2007, Variety of stylolites' morphologies and
576 statistical characterization of the amount of heterogeneities in the rock: Journal of Structural
577 Geology, v. 29, p. 422-434, http://doi.org/10.1016/j.jsg.2006.09.014.

578 Brunet, M.F., and Le Pichon, X., 1982, Subsidence of the Paris basin: Journal of Geophysical Research:
579 Solid Earth, v. 87, p. 8547-8560.

580 Bruna, P.O., Lavenu, A.P., Matonti, C. and Bertotti, G., 2018, Are stylolites fluid-flow efficient
581 features?: Journal of Structural Geology, https://doi.org/10.1016/j.jsg.2018.05.018 (in press)

582 Candela, T., Renard, F., Bouchon, M., Brouste, A., Marsan, D., Schmittbuhl, J, and Voisin, C., 2009,
583 Characterization of Fault roughness at various scales : implication of three dimensional high
584 resolution topography measurements. In: Ben-Zion, Y., and Sammis, C., (eds.): Mechanics,
585 Structurre and Evolution of Fault Zones, Birkhauser Basel, p. 1817-1851.

586 Croizé, D., Renard, F., Bjørlykke, K., and Dysthe, D.K., 2010, Experimental calcite dissolution under
587 stress: Evolution of grain contact microstructure during pressure solution creep: Journal of
588 Geophysical Research: Solid Earth, v. 115, B09207, http://doi.org/10.1029/2010jb000869.

589 Dassié, E.P., Genty, D., Noret, A., Mangenot, X., Massault, M., Lebas, N., Duhamel, M., Bonifacie, M.,
590 Gasparrini, M., Minster, B., and Michelot, J.-L., 2018, A newly designed analytical line to
591 examine fluid inclusion isotopic compositions in a variety of carbonate samples:
592 Geochemistry, Geophysics, Geosystems, v. 19,p. 1107–1122.
593 http://doi.org/10.1002/2017GC007289

594 Delmas, J., Houel, P., and Vially, R., 2002, Paris Basin, Petroleum potential: IFP regional Report.

595 Delmas, J., Brosse, E., and Houel, P., 2010, Petrophysical properties of the middle jurassic carbonates
596 in the PICOREF Sector (South Champagne, Paris Basin, France): Oil and Gas Science and
597 Technology–Revue de l'Institut Français du Pétrole, v. 65, p. 405-434.

598 Dunham, R.J., 1962, Classification of carbonate rocks according to depositional textures, *in*: Ham,
599 W.E., ed., Classification of Carbonate Rocks, AAPG [Tulsa], p. 108 – 121.

600 Dunnington, H.V., 1967, Aspects of Diagenesis and Shape Change in Stylolitic Limestone Reservoirs:
601 World Petroleum Congr. Proc., Mexico, vol. 2, pp. 339–352.

602 Ebner, M., Koehn, D., Toussaint, R., and Renard, F., 2009a, The influence of rock heterogeneity on the
603 scaling properties of simulated and natural stylolites: Journal of Structural Geology, v. 31, p.
604 72-82, http://doi.org/10.1016/j.jsg.2008.10.004.

605 Ebner, M., Koehn, D., Toussaint, R., Renard, F., and Schmittbuhl, J., 2009b, Stress sensitivity of stylolite
606 morphology: Earth and Planetary Science Letters, v. 277, p. 394-398,
607 http://doi.org/10.1016/j.epsl.2008.11.001.

608 Ebner, M., Piazolo, S., Renard, F., and Koehn, D., 2010a, Stylolite interfaces and surrounding matrix
609 material: Nature and role of heterogeneities in roughness and microstructural development:
610 Journal of Structural Geology, v. 32, p. 1070-1084, http://doi.org/10.1016/j.jsg.2010.06.014.

611 Ebner, M., Toussaint, R., Schmittbuhl, J., Koehn, D., and Bons, P., 2010b, Anisotropic scaling of
612 tectonic stylolites: A fossilized signature of the stress field?: Journal of Geophysical Research,
613 v. 115, B06403, http://doi.org/10.1029/2009jb006649.

614 Ehrenberg, S., 2006. Porosity destruction in carbonate platforms: Journal of Petroleum Geology, v.
615 29, p. 41-52.

616 Ehrenberg, S.N., Eberli, G.P., Keramati, M., and Moallemi, S.A., 2006, Porosity-permeability
617 relationships in interlayered limestone-dolostone reservoirs: AAPG Bulletin, v. 90, p. 91-114,
618 http://doi.org/10.1306/08100505087.

619 Espitalié, J., Maxwell, J., Chenet, Y., and Marquis, F., 1988, Aspects of hydrocarbon migration in the
620 Mesozoic in the Paris Basin as deduced from an organic geochemical survey: Organic
621 Geochemistry, v. 13, p. 467-481.

622 Finkel, E.A., Wilkinson, B.H., 1990, Stylolitization as a source of cement in Mississippian Salem
623 limestone, West-Central Indiana: AAPG Bull, v. 74, p. 174–186.

624 Fletcher, R.C., and Pollard, D.D., 1981, Anticrack model for pressure solution surfaces: Geology, v. 9,
625 p. 419-424, http://doi.org/10.1130/0091-7613(1981)9<419:amfpss>2.0.co;2.

626 Garcia, J.-P., 1993, Les variations du niveau marin sur le bassin de Paris au Bathonien-Callovien.
627 Impacts sur les communautés benthiques et sur l'évolution des Ornithellidés
628 (Terebratellinida). Mémoires Géologiques de l'Université de Dijon, 310 p.

629 Garcia, J.-P., and Sambet, 1994, Macrobenthic associations as a biostratigraphical tool for high
630 resolution correlations within mixed siliciclastic/carbonates sequences (Middle Jurassic, Paris
631 Basin). Book of abstracts "High resolution sequence stratigraphy: innovations and
632 applications", Liverpool - p. 283-287.

633 Gaumet, F., 1994, Stratigraphie séquentielle haute resolution en milieu carbonaté: l´exemple de la

634 plate-forme Bourguignonne au Bathonien et au Callovien [Ms Thesis] : Université de Dijon, 50 p.

635 Gaumet, F., 1997, Fondements géologiques pour la modélisation stratigraphique des systèmes
636 carbonatés: le jurassique moyen de l'Angleterre à la Méditerranée [PhD Thesis] : Université
637 C. Bernard – Lyon, 290 p.

638 Gaumet, F., Garcia, J.-P., Dromart, G., and Sambet, G., 1996, Contrôle stratigraphique des faciès,
639 géométries et profils de dépôt de la plate-forme carbonatée bourguignonne au Bathonien-
640 Callovien : Bulletin de la Société géologique de France, v. 167, p. 409-421.

641 Granier, B., 1995, A sedimentological model of the Callovian oolite reservoir of the Villeperdue oil
642 field, Paris Basin (France): TOTAL Exploration Production, Scientific and Technical Center, p.
643 145-150.

644 Gratier, J.P., Muquet, L., Hassani, R., and Renard, F., 2005, Experimental microstylolites in quartz and
645 modeled application to natural stylolitic structures: Journal of Structural Geology, v. 27, p.
646 89-100, http://doi.org/10.1016/j.jsg.2004.05.007.

647 Guillocheau, F., Robin, C., Allemand, P., Bourquin, S., Brault, N., Dromart, G., Friedenberg, R., Garcia,
648 J.-P., Gaulier, J.M., Gaumet, F., Grosdoy, B., Hanot, F., Le Strat, P. et al. 2000. Meso-Cenozoic
649 geodynamic evolution of the Paris Basin: 3D stratigraphic constraints. Geodinamica Acta, 13,
650 189-245.

651 Guillocheau, F. 1991. Mise en évidence de grands cycles transgression-régression d'origine tectonique
652 dans les sédiments mésozoiqies du Bassin de Paris. C.R. Académie des Sciences de Paris, 312,
653 1687-1593.

654 Hassan, H.M. 2007. Stylolite effect on geochemistry, porosity and permeability: Comparison between
655 a limestone and a dolomite sample from Khuff-B reservoir in Eastern Saudi Arabia. The
656 Arabian Journal of Science and Engineering, 32, 10.

657 Heap, M.J., Baud, P., Reuschle, T. and Meredith, P.G. 2013. Stylolites in limestones: Barriers to fluid
658 flow? Geology, 42, 51-54, http://doi.org/10.1130/g34900.1.

659 Homewood, P., Guillocheau, F., Eschard, R., and Cross, T, 1992, Corrélation haute resolution et
660 stratigraphie génétique: une demarche intégrée : Bull. Centres Rech. Explor. – Prod. Elf-
661 Aquitaine, Boussens, v. 16, p. 357-381.

662 Karcz, Z. and Scholz, C.H. 2003. The fractal geometry of some stylolites from the Calcare Massiccio
663 Formation, Italy. Journal of Structural Geology, 25, 1301-1316,
664 http://doi.org/10.1016/s0191-8141(02)00173-6.

665 Kelka, U., Veveakis, M., Koehn, D. and Beaudoin, N. 2017. Zebra rocks: compaction waves create ore
666 deposits: Scientific reports, 7, 14260.

667 Khair, H.A., Cooke, D. and Hand, M. 2013. The effect of present day in situ stresses and paleo-stresses
668 on locating sweet spots in unconventional reservoirs, a case study from Moomba-Big Lake
669 fields, Cooper Basin, South Australia. Journal of Petroleum Exploration and Production
670 Technology, 3, 207-221.

671 Khair, H.A., Cooke, D. and Hand, M. 2015. Seismic mapping and geomechanical analyses of faults
672 within deep hot granites, a workflow for enhanced geothermal system projects. Geothermics,
673 53, 46-56.

674 Koehn, D., Renard, F., Toussaint, R. and Passchier, C. 2007. Growth of stylolite teeth patterns
675 depending on normal stress and finite compaction. Earth and Planetary Science Letters, 257,
676 582-595, http://doi.org/10.1016/j.epsl.2007.03.015.

677 Koehn, D., Ebner, M., Renard, F., Toussaint, R. and Passchier, C.W. 2012. Modelling of stylolite
678 geometries and stress scaling. Earth and Planetary Science Letters, 341-344, 104-113,
679 http://doi.org/10.1016/j.epsl.2012.04.046.

680 Koehn, D., Rood, M.P., Beaudoin, N., Chung, P., Bons, P.D. and Gomez-Rivas, E. 2016. A new stylolite
681 classification scheme to estimate compaction and local permeability variations. Sedimentary
682 Geology, 346, 60-71, http://doi.org/10.1016/j.sedgeo.2016.10.007.

683 Koepnick, R. 1987. Distribution and permeability of stylolite-bearing horizons within a Lower
684 Cretaceous carbonate reservoir in the Middle East. SPE Formation Evaluation, 2, 137-142.

685 Lacombe, O., Laurent, P. and Angelier, J. 1994. Calcite twins as a key to paleostresses in sedimentary
686 basins: Preliminary results from drill cores of the Paris basin. Peri-Tethyan Platforms, F. Roure
687 Ed.: Technip, 197-210.

688 Lacombe, O., Angelier, J., Byrne, D. and Dupin, J. 1993. Eocene-Oligocene tectonics and kinematics of
689 the Rhine-Saone Continental Transform Zone (eastern France). Tectonics, 12, 874-888.

690 Lacombe, O., Angelier, J., Laurent, P., Bergerat, F. and Tourneret, C. 1990. Joint analyses of calcite
691 twins and fault slips as a key for deciphering polyphase tectonics: Burgundy as a case study.
692 Tectonophysics, 182, 279-300.

693 Laronne Ben-Itzhak, L., Aharonov, E., Karcz, Z., Kaduri, M. and Toussaint, R. 2014. Sedimentary
694 stylolite networks and connectivity in limestone: Large-scale field observations and
695 implications for structure evolution. Journal of Structural Geology, 63, 106-123,
696 http://doi.org/10.1016/j.jsg.2014.02.010.

697 Le Solleuz, A., Doin, M.-P., Robin, C. and Guillocheau, F. 2004. From a mountain belt collapse to a
698 sedimentary basin development: 2-D thermal model based on inversion of stratigraphic data
699 in the Paris Basin. Tectonophysics, 386, 1-27.

700 Mangenot, X., Gasparrini, M., Rouchon, V. and Bonifacie, M. 2018. Basin-scale thermal and fluid flow
701 histories revealed by carbonate clumped isotopes (Δ_{47})–Middle Jurassic carbonates of the
702 Paris Basin depocentre. Sedimentology, 65, 123-150.

703 Mangenot, X., Bonifacie, M., Gasparrini, M., Götz, A., Ader M., Rouchon, V., 2017. Coupling Δ_{47} and
704 fluid inclusion thermometry on carbonate cements to precisely reconstruct the temperature,
705 salinity and $\delta^{18}O$ of paleo-groundwater in sedimentary basins. Chemical Geology, 472: 44-57.
706 DOI: 10.1016/j.chemgeo.2017.10.011

707 Mangenot, X., Gasparrini, M., Bonifacie, M., Gerdes, A. and Rouchon, V. 2017. An emerging thermo-
708 chronometer to resolve longstanding enigmas in sedimentary basin analysis - Δ_{47}/(U-Pb).
709 Goldschmidt, Paris.

710 Martín-Martín, J., Gomez-Rivas, E., Gómez-Gras, D., Travé, A., Ameneiro, R., Koehn, D. and Bons, P.
711 2018. Activation of stylolites as conduits for overpressured fluid flow in dolomitized platform
712 carbonates. Geological Society, London, Special Publications, 459, 157-176.

713 Meredith, P.G., Baud, P., Heap, M.J., Rolland, A. and Toussaint, R. 2011. Influence of compaction
714 bands and stylolites on the permeability of porous rocks. Flows and mechanics in natural
715 porous media from pore to field scale. Pore2Field, Reuil-Malmaison, 4.

716 Merino, E., Ortoleva, P. and Strickholm, P. 1983. Generation of evenly-spaced pressure-solution
717 seams during (late) diagenesis: A kinetic theory. Contributions to Mineralogy and Petrology,
718 82, 360-370.

719 Nicolaides, S., Wallace, M.W., 1997, Pressure dissolution and cementation in an Oligotropical
720 limestone (Clifton Formation), Otway Basin, Australia: In: James, N.P., Clarke, J.A.D. (Eds.),
721 Cool Water Carbonates. SEPM Spec.Publ., v. 56, p. 249–261.

722 Oelkers, E.H., Bjørkum, P. and Murphy, W.M. 1996. A petrographic and computational investigation
723 of quartz cementation and porosity reduction in North Sea sandstones. American Journal of
724 Science, 296, 420-452.

725 Peacock, D.C.P. and Azzam, I.N. 2006. Development and scaling relationships of a stylolite population.
726 Journal of Structural Geology, 28, 1883-1889, http://doi.org/10.1016/j.jsg.2006.04.008.

727 Perrodon, A. and Zabek, J. 1990. Paris Basin: Chapter 32: Part II. Selected Analog Interior Cratonic
728 Basins: Analog Basins.

729 Railsback, L.B., 1993, Contrasting styles of chemical compaction in the Upper Pennsylvanian Dennis
730 limestone in the Midcontinent region, USA: I. Sed. Petrol, v. 63,p. 61–72.

731 Raynaud, S. and Carrio-Schaffhauser, E. 1992. Rock matrix structures in a zone influenced by a
732 stylolite. Journal of Structural Geology, 14, 973-980.

733 Renard, F. 2004. Three-dimensional roughness of stylolites in limestones. Journal of Geophysical
734 Research, 109, http://doi.org/10.1029/2003jb002555.

735 Renard, F., Dysthe, D., Feder, J., Bjørlykke, K. and Jamtveit, B. 2001. Enhanced pressure solution creep
736 rates induced by clay particles: Experimental evidence in salt aggregates. Geophysical
737 Research Letters, 28, 1295-1298.

738 Rolland, A., Toussaint, R., Baud, P., Conil, N. and Landrein, P. 2014. Morphological analysis of stylolites
739 for paleostress estimation in limestones. International Journal of Rock Mechanics and Mining
740 Sciences, 67, 212-225, http://doi.org/10.1016/j.ijrmms.2013.08.021.

741 Schmittbuhl, J., Renard, F., Gratier, J.P. and Toussaint, R. 2004. Roughness of stylolites: implications
742 of 3D high resolution topography measurements. Phys Rev Lett, 93, 238501,
743 http://doi.org/10.1103/PhysRevLett.93.238501.

744 Shinn, E.A. and Robbin, D.M. 1983. Mechanical and chemical compaction in fine-grained shallow-
745 water limestones. Journal of Sedimentary Research, 53.

746 Simonsen, I., Vandembroucq, D. and Roux, S. 2000. Wave scattering from self-affine surfaces. Physical
747 Review E, 61, 5914.

748 Sinha-Roy, S. 2002. Kinetics of differentiated stylolite formation. Current Science, 82, 9.

749 Tavani, S., Storti, F., Fernández, O., Muñoz, J.A., and Salvini, F., 2006. 3-D deformation pattern analysis
750 and evolution of the Añisclo anticline, southern Pyrenees: Journal of Structural Geology, 28,
751 695-712.

752 Tavani, S., Storti, F., Lacombe, O., Corradetti, A., Muñoz, J.A., and Mazzoli, S., 2015. A review of
753 deformation pattern templates in foreland basin systems and fold-and-thrust belts:
754 Implications for the state of stress in the frontal regions of thrust wedges: Earth-Science
755 Reviews, 141, 82-104.

Teles, V., Fornel, A., Houel, P., Delmas, J., Mengus, J., Michel, A., and Maurand, N., 2014. Coupling basin and reservoir simulators for an improved CO2 injection flow model: Energy Procedia, 63, 3665-3675.

Torelli, M. 2018. 3D modelling of the Paris basin petroleum system. IFP Energies nouvelles Report n° A0250887, 75 pp.

Toussaint, R., Aharonov, E., Koehn, D., Gratier, J. P., Ebner, M., Baud, P., Rolland, A., and Renard, F., 2018. Stylolites: A review: Journal of Structural Geology, 114, 163-195.

Vandeginste, V. and John, C.M. 2013. Diagenetic implications of stylolitization in pelagic carbonates, Canterbury Basin, offshore New Zealand. Journal of Sedimentary Research, 83, 226-240.

Walderhaug, O., Bjorkum, P.A. and Aase, N.E. 2006. Kaolin-coating of stylolites, effect on quartz cementation and general implications for dissolution at mineral interfaces. Journal of Sedimentary Research, 76, 234-243.

Wendebourg, J. and Lamiraux, C. 2002. Estimating the ultimate recoverable reserves of the Paris Basin, France. Oil and gas science and technology, 57, 621-629.

771 Table 1 – Results of the Stylolite Roughness Inversion Technique (SRIT).

772

773 Figures captions

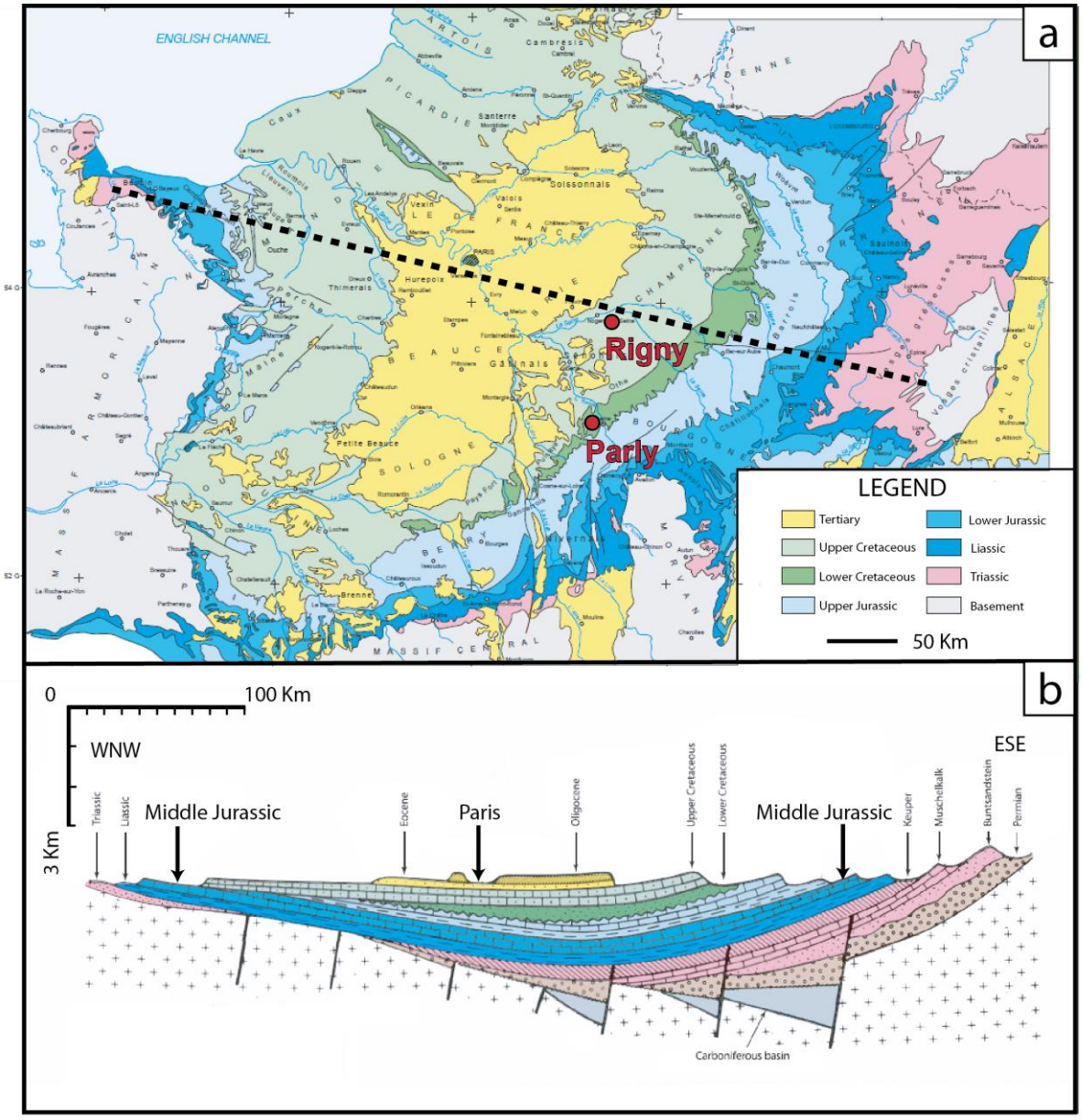

774

775 Figure 1 – a) Geological map of the Paris basin with the location of the studied cores (Rigny and Parly,
776 from depocenter and southern margin, respectively), and the WNW-ESE cross-section displayed below
777 in b). Modified after Perrodon and Zabeck (1991) and Delmas et al. (2002).

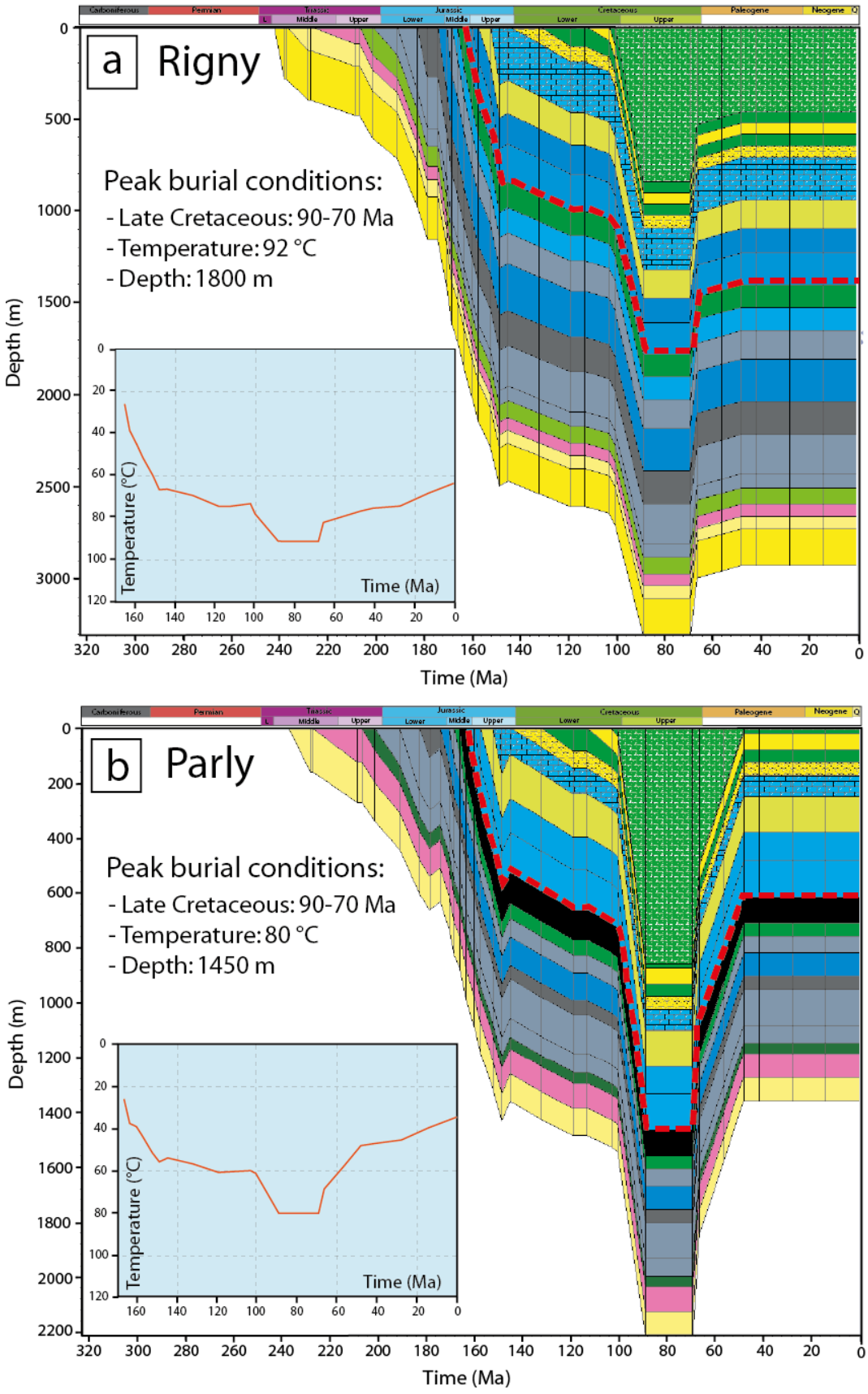

778

779 Figure 2 – 1D burial curves extracted from the Paris basin 3D basin model for the two studied wells,
780 which describe the evolution of depth with time for the different stratigraphic intervals. The red

781 dotted lines indicate the location of the studied Middle Jurassic (Upper Bathonian – Lower Callovian)
782 interval. The temperature evolution with time of these rocks is reported in the graphs. a) Rigny
783 (depocentre) ; b) Parly (southern margin).

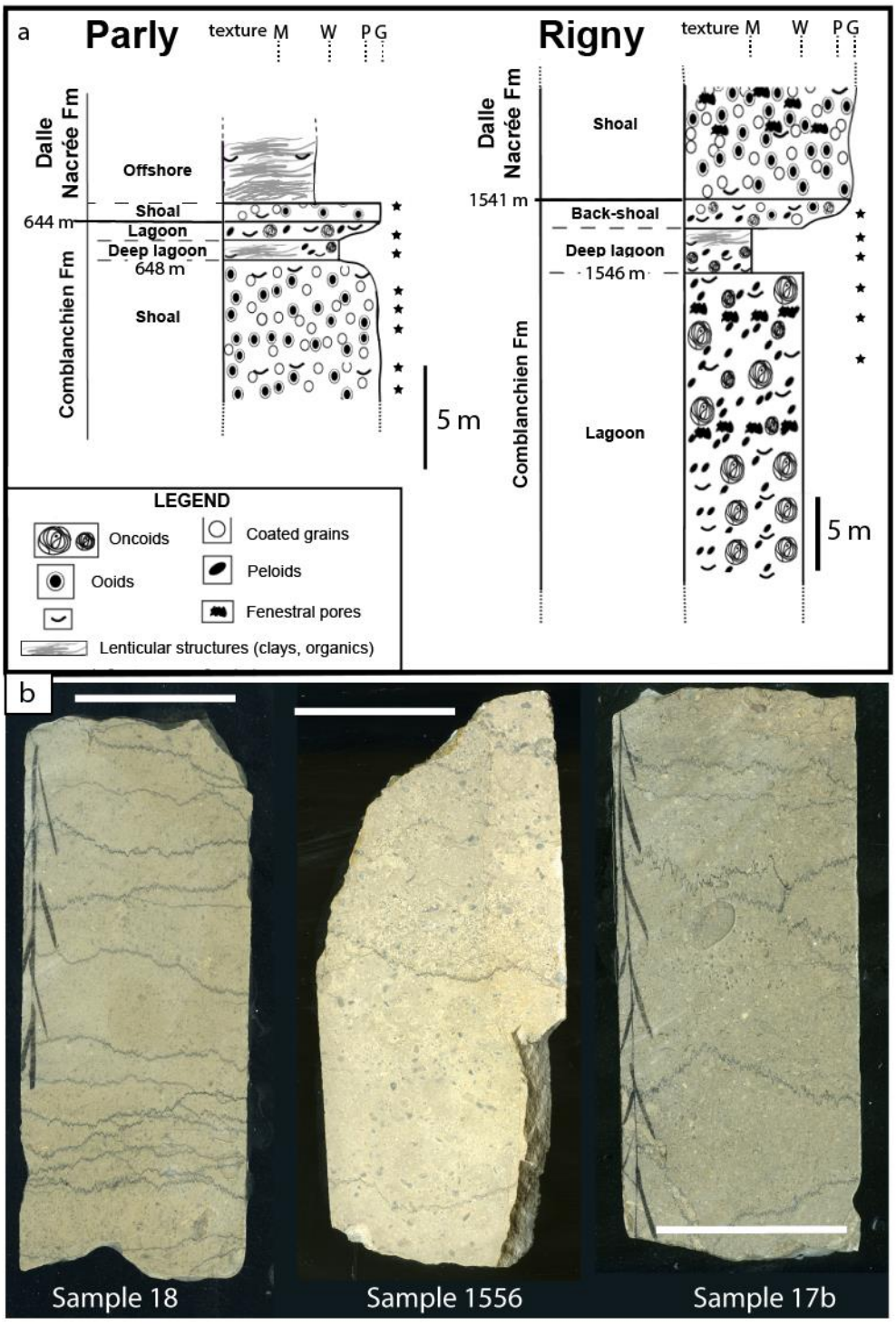

784

785 Figure 3 - a) Simplified stratigraphic columns for the Rigny and Parly core sections investigated, with
786 the depositional environments reconstructed by macro- and micro-facies analysis. Horizontal

thickness of the column indicates the carbonate dominant texture of the different depositional environments also illustrated in Figure 4. The texture code is as follow: M: Mudstone, W:Wackstone; P: Packstone; G: Grainstone. Asterisks locate the samples used in this study. b) examples of core samples investigated, exhibiting various density and morphology of stylolites. White scale bars represent 5 cm.

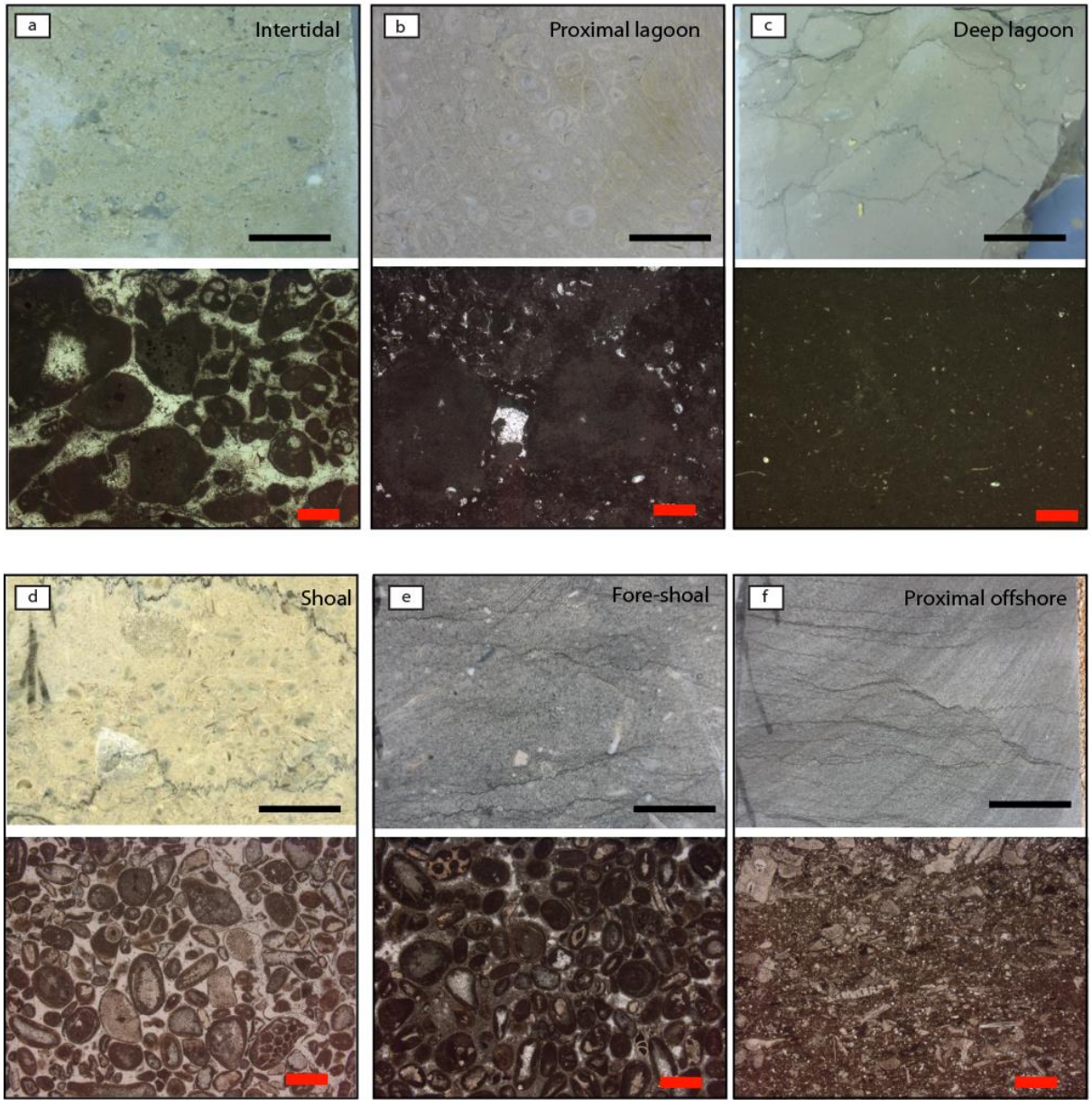

Fig. 4 - Example of macro-facies (top, scanned hand-sample) and micro-facies (bottom, optical microphotograph) and corresponding depositional environments. a) Grainstone with oncoids in a

groundmass of fine intraclasts and fenestral pores cemented by calcite (intertidal). b) Floatstone with large oncoids (proximal lagoon). c) Highly bioturbated mudstone (deep lagoon). d) Grainstone with coated grains, bioclasts and ooids (shoal). e) Packstone with ooids and large crinoid fragments (fore-shoal). f) Fine packstone to wackstone alternated with marly layers containing crinoid and brachiopod fragments (proximal off-shore). Red and black scale bars are 2 cm.

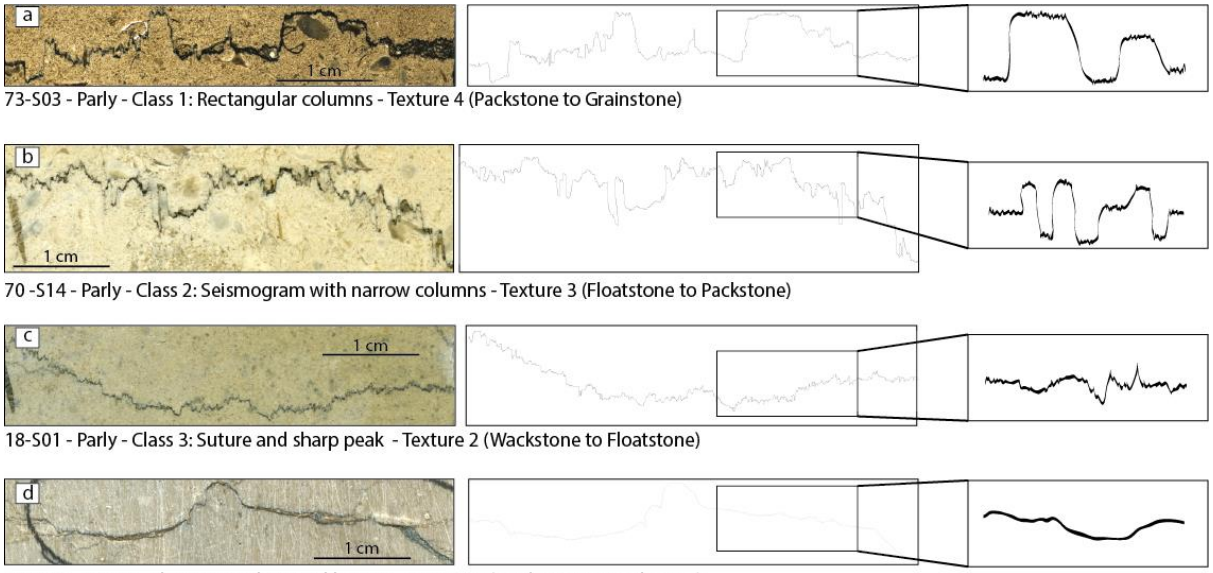

Figure 5 – a-d) Examples of stylolite classes based on morphology as proposed by Koehn et al. (2016), with high resolution scan (left-hand side), stylolite track drawn for SRIT (middle) and sketch showing general morphology class characteristics (right-hand side).

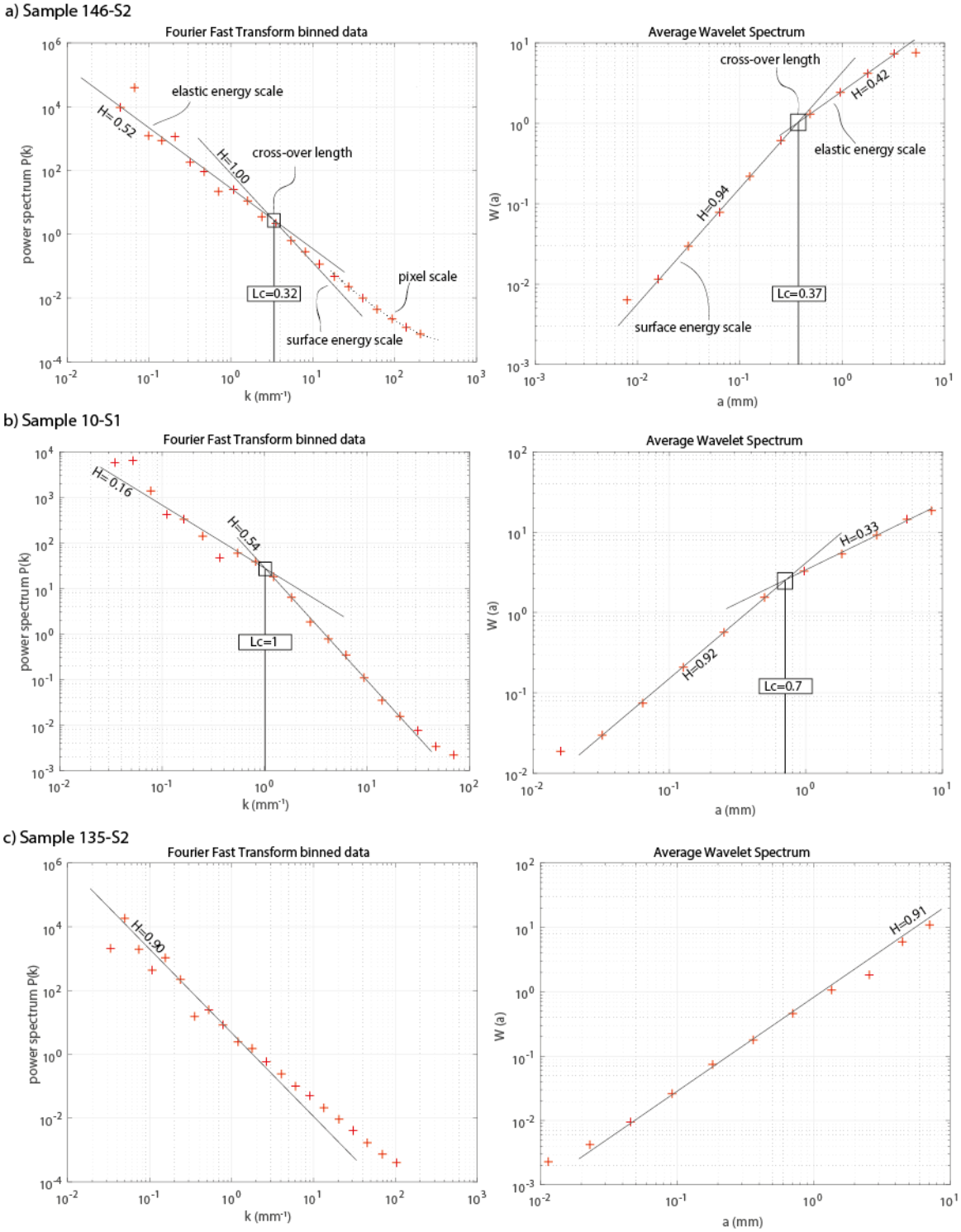

804

805 Figure 6 – Fourier Power Spectrum (left-hand side) and Average Wavelet Coefficient (right-hand side)
806 log-log plot obtained from 3 different BPS tracks. Data are represented as red crosses. Straight lines
807 representing growth regimes are reported in black with corresponding Hurst coefficient values (H)
808 calculated, and cross-over values (Lc) obtained from intersection (if any) between both lines are
809 reported in mm in the black frame.

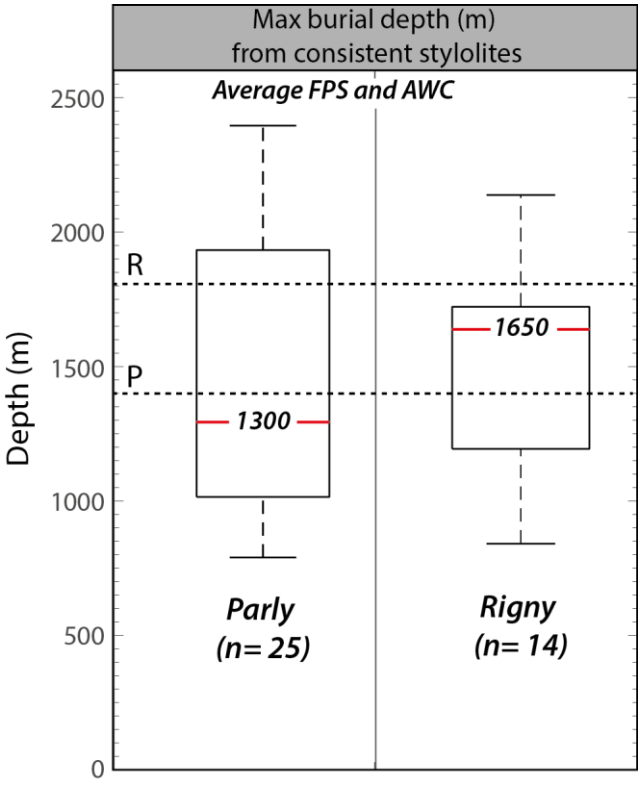

Figure 7 – Box-and-whisker plots of the burial depth derived from magnitude of vertical stress obtained from SRIT for each core, considering only the BPS that are consistent (see text for details). Distribution is reported as horizontal lines from bottom to top: the minimum value in the population, the first quartile, the median value (red line), the third quartile, and the maximum value of the population. Values of the medians (red line) are reported on the plot. Dotted lines represent the maximum burial depths predicted independently from basin modeling for the two cores (P: Parly, R: Rigny).

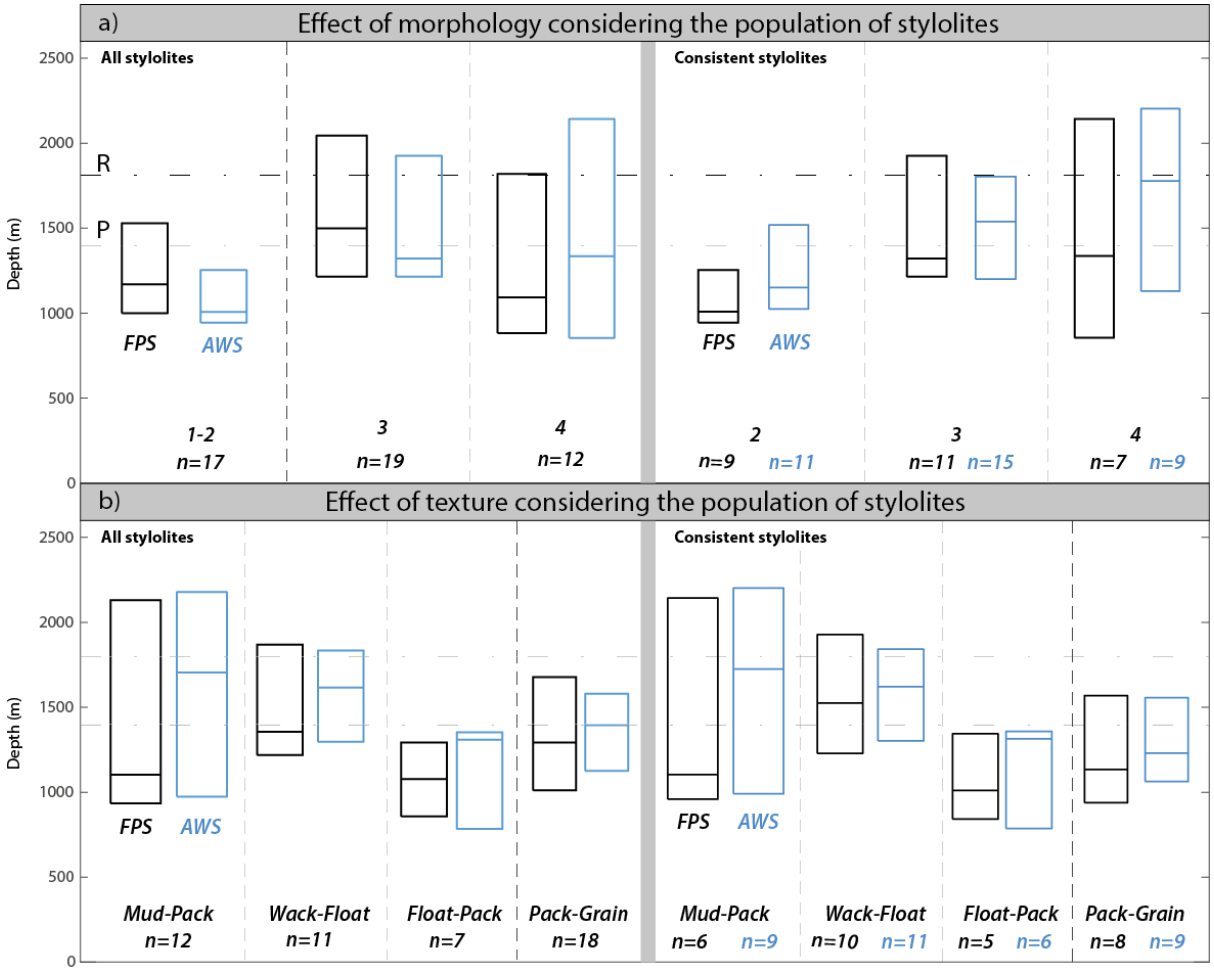

Figure 8 – Box-and-whisker plots reporting the magnitude of the vertical stress obtained from SRIT applied to the population of BPS considering both cores as one, reporting as horizontal lines from bottom to top: the first quartile, the median value, and the third quartile. Black box plots (left-hand side of each plot) result from Fourier Power Spectrum (FPS) analysis, whereas blue box plots (right-hand side of each plot) result from Average Wavelet Coefficient (AWS) method. Dotted lines represent the maximum burial depth predicted independently from basin modelling for the two cores (P: Parly, R: Rigny). a) Population divided regarding the stylolite morphology (2: Seismogram, 3: Suture and sharp peak, 4: Simple wave), considering the whole population (left-hand side) and only the consistent data (right-hand side). b) Population divided regarding the carbonate texture (1: Mudstone to wackstone, 2: Wackstone to floatstone, 3: Floatstone to Packstone, 4: Packstone to grainstone), considering the whole population (left-hand side) and only the stylolite giving consistent Hurst exponent (right-hand side).

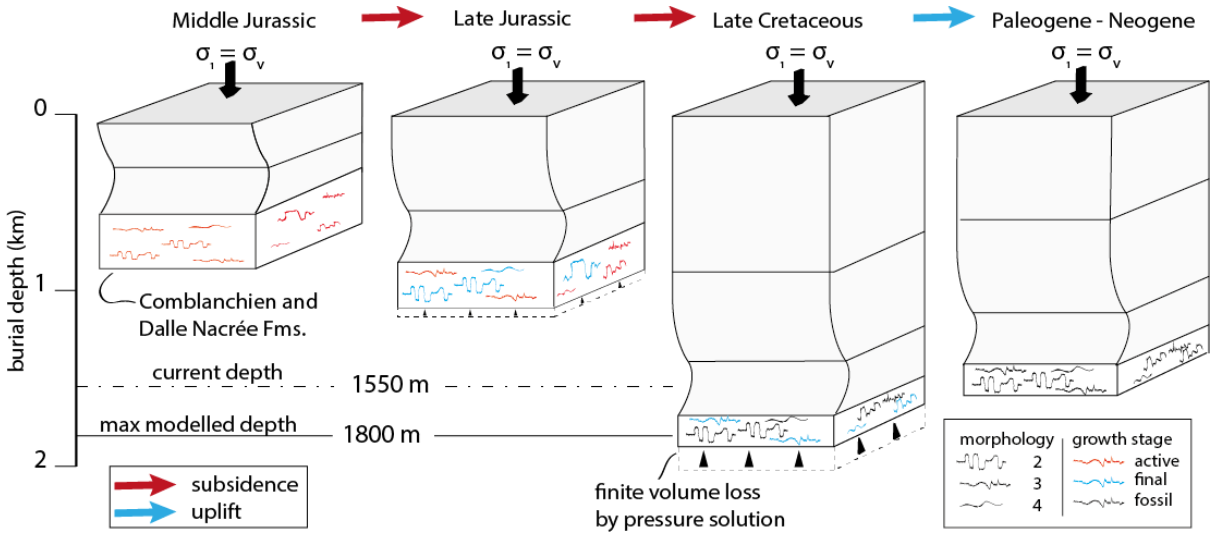

Figure 9 – Schematic representation of the bedding-parallel stylolite (BPS) growth at different steps of the host rock burial history, based on the findings from the Paris basin depocentre (Rigny core). Stylolites of different morphology classes are represented only in the studied Middle Jurassic interval (white stratum). Sediments successively piled up are represented by the grey strata. Stylolites of classes 2, 3 and 4 are pictured in colours depending if the growth is active (red), final (blue), or fossil (black). Current burial depth and maximum burial depth are derived respectively from the well drilling report and the burial-thermal modelling for the Rigny core. Final stage of BPS growth (in blue) is represented in accordance with the results of the roughness inversion reported on Figure 8.